



Stationarity Evaluation of High-mobility sub-6 GHz and mmWave non-WSSUS Channels

Danilo Radovic^{*(1)}, Faruk Pasic⁽¹⁾, Markus Hofer⁽²⁾, Herbert Groll⁽¹⁾, Christoph F. Mecklenbräucker⁽¹⁾, and Thomas Zemen⁽²⁾

(1) TU Wien, Vienna, Austria; e-mail: danilo.radovic@tuwien.ac.at

(2) AIT Austrian Institute of Technology GmbH, Vienna

Abstract

Analysis and modeling of wireless communication systems are dependent on the validity of the wide-sense stationarity uncorrelated scattering (WSSUS) assumption. However, in high-mobility scenarios, the WSSUS assumption is approximately fulfilled just over a short time period. This paper focuses on the stationarity evaluation of high-mobility multi-band channels. We evaluate the stationarity time, the time over which WSSUS is fulfilled approximately. The investigation is performed over real, measured high-mobility channels for two frequency bands, 2.55 and 25.5 GHz. Furthermore, we demonstrate the influence of the user velocity on the stationarity time. We show that the stationarity time decreases with increased relative velocity between the transmitter and the receiver. Furthermore, we show the similarity of the stationarity regions between sub-6 GHz and mmWave channels. Finally, we demonstrate that the sub-6 GHz channels are characterized by longer stationarity time.

1 Introduction

High-mobility communication is gaining momentum in the vehicular domain, high-speed railways, uncrewed aerial vehicles (UAVs) communications, etc. However, in order to offer reliable data communication, further understanding of high-mobility wireless channels is required. Furthermore, channel modeling is dependent on the exact characterizations of the actual, measured channels. Since the communication participants are moving at a high velocity, we have to deal with rapidly changing propagation conditions. Therefore, the validity of the wide-sense stationarity uncorrelated scattering (WSSUS) assumption is limited in both time and frequency. Furthermore, capacity requirements introduce a heavy burden on the crowded sub-6 GHz spectrum. As a possible solution, data offloading in a less characterized millimeter wave (mmWave) spectrum is proposed. Hence,

The work of D.Radovic and F.Pasic was supported by the Austrian Research Promotion Agency (FFG) via the research project Intelligent Intersection (ICT of the Future, Grant 880830). The work of M. Hofer and T. Zemen was supported by the project DEDICATE (Principal Scientist grant) at the AIT Austrian Institute of Technology.

in this paper, we compare the stationarity characteristics of multiband measurements, at 2.55 and 25.5 GHz. It is essential to determine the maximal time duration over which the WSSUS assumption is approximately satisfied. We define this time duration as stationarity time.

The theoretical approach of statistical characterization of non-WSSUS channels is given in [1, 2]. The author introduces time-frequency (TF) dependent power spectrum representation, known as local scattering function (LSF). Furthermore, the author defines the WSSUS as satisfied as long as the LSF is constant over a given time and frequency range. Multiple works analyze the stationarity of measured sub-6 GHz wireless channels, [3, 4, 5, 6]. They conclude that the minimum stationarity region is on the order of 40 ms in the time domain. The authors of [6] investigate the influence of the communication participants' velocity on the stationarity time. Based on the measurements, they argue that higher relative speed lowers the stationarity time. First stationarity evaluations of high-mobility mmWave channels are provided in [7, 8]. [7] analyzes the stationarity time of 28 GHz channels in highway environment. Their results demonstrate the stationarity time in the range of 2-9 ms, when the relative speed between TX and RX is 100 km/h. The authors of [8] show stationarity time of 5-16 ms for an 60 GHz urban scenario and the relative speed of 56 km/h. Finally, [9] evaluates multi-band stationarity in a static environment. The authors demonstrate that the channels with a center frequency above 6 GHz are characterized by shorter spatial stationarity regions, than conventional channels in the sub-6 GHz spectrum.

Contributions of the paper: In this paper we present channel stationarity evaluation of measured high-speed channels. To our best knowledge, this work presents the first stationarity evaluation of real channels, obtained by repeatable measurements. Repeatable measurements mean that we measure the channel multiple times (where we vary a specific parameter), while moving along the exact same path, and the scattering environment stays constant. Therefore, it enables us to differentiate between the impacts of individual parameters (movement velocity and center frequency). To the best of our knowledge, we present the first evaluation of the influence of the participants' velocity on the distribution of the mmWave spatial stationarity, and

the length of the stationarity time. Secondly, we provide a comparison of the channel stationarity for sub-6 GHz and mmWave channels.

2 Measurement Setup

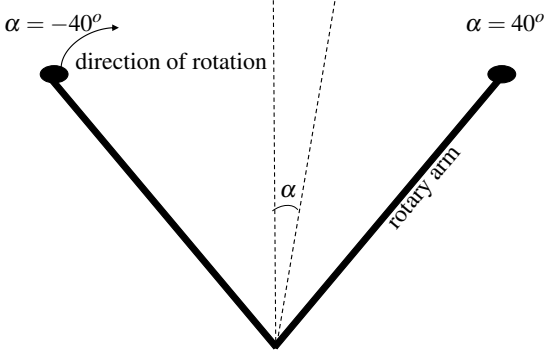


Figure 1. Measurement setup: TX defined movement.

In this paper we evaluate measured high-mobility channels. The measurement campaign is performed in a controlled indoor lab scenario. The transmitter is placed on a 1 m long rotary arm (Fig. 1). The measurement is performed once the rotary arm achieves a constant velocity. For each scenario, the channel is measured along the exactly same path, as the rotary arm moves from $\alpha = -40^\circ$ to $\alpha = 40^\circ$ angle relative to the vertical axis. For the multi-band measurements, different transmit antennas are placed at the exact same position. The receiver is fixed in the neighboring room 8 m away from the transmitter. This setup enables a fair comparison between sub-6 GHz and mmWave systems in terms of small-scale and fast-fading in a high-mobility scenario. In each scenario bandwidth $B = 100$ MHz is set, and contains 500 channel measurements in the time domain. In order to keep a constant number of time samples the subcarrier spacing is set to 400 kHz and 1 MHz for the velocity 40 km/h and 100 km/h, respectively. In this paper we evaluate the measured channel at 2.55 GHz and 25.5 GHz and velocity 40 km/h and 100 km/h. The measurement setup is explained in detail in [10, 11].

3 Stationarity evaluation

The measured channel, described in Section 2, is defined by its time-variant channel transfer function

$$H[s, q] = H(sT_s, qf_s), \quad (1)$$

where $s \in [1, \dots, S]$ are time and $q \in [1, \dots, Q]$ frequency indices, and T_s and f_s sampling time and frequency. Since the high-mobility channels are non-WSSUS, we define the TF subregions, over which we assume stationarity. We denote these regions as local channel transfer function (LCTF) $\mathbf{H}_{k_t}[s', q']$, spanning over NT_s and Mf_s length in time and frequency, respectively. s' and q' are local time and frequency indices and k_t denotes the index of each local region

$$k_t \in [1, \dots, K_t], \quad K_t = \left\lfloor \frac{S - N}{\Delta_t} \right\rfloor + 1, \quad (2)$$

with time shift $\Delta_t T_s$ between two consecutive LCTFs. When choosing N we have to find a trade-off between the accuracy of stationary evaluation and LSF Doppler resolution. By increasing N , we risk violating the stationarity assumption, but gain the LSF Doppler resolution, which is inversely proportional to NT_s . The channel is measured over a bandwidth of 100 MHz, leading to a delay resolution of 10 ns. Hence, we assume stationarity over the whole bandwidth and focus on determining the stationarity time. When calculating the LSF, we aim to minimize the variance of the spectral estimate. Therefore, we use a multitaper spectral estimator by applying two-dimensional spectral window functions, $G_w[s', q'] = u_i[s']\tilde{u}_j[q']$, which generates TF limited spectral estimates with low sidelobes, as given in [12]. \mathbf{u}_i and $\tilde{\mathbf{u}}_j$ are discrete prolate spheroidal sequence (DPSS), described by its energy concentration bandwidth ($2W_t$, $2W_f$), and the number of sequences (I , J), in the time and frequency domain. Here, we deal with a trade-off between the spectral resolution and sidelobe level. We set the $W_t = 2$, $I = 2$ and $W_f = 1$, $J = 1$ DPSS parameters in the time and frequency domain, respectively. Further, we define the windowed channel transfer

$$\hat{\mathbf{H}}_{k_t}^{(G_w)} = \mathbf{H}_{k_t} \odot \mathbf{G}_w, \quad (3)$$

where \odot denotes the Hadamard product. Next, we obtain the windowed Doppler-variant impulse response

$$\hat{\mathbf{S}}_{k_t}^{(G_w)} = \mathbf{F}_N \hat{\mathbf{H}}_{k_t}^{(G_w)} \mathbf{F}_M^H, \quad (4)$$

\mathbf{F}_i and \mathbf{F}_i^H representing discrete Fourier transform (DFT) and inverse DFT (IDFT) matrix of size i . We calculate the LSF by applying uniform weighting across the IJ windowed Doppler-variant impulse responses

$$\hat{\mathbf{C}}_{k_t} = \frac{1}{IJ} \sum_{w=1}^{IJ} \left| \hat{\mathbf{S}}_{k_t}^{(G_w)} \right|^2. \quad (5)$$

We define the channel stationarity region as a time period over which the LSF is approximately constant. Therefore, we perform a dual-time LSF comparison employing the collinearity spectral distance metric

$$\gamma^{(t)}[k_t, k_{\Delta t}] = \frac{\langle \hat{\mathbf{C}}_{k_t}, \hat{\mathbf{C}}_{k_{\Delta t}} \rangle_{\mathbf{F}}}{\sqrt{\|\hat{\mathbf{C}}_{k_t}\|_{\mathbf{F}}^2 \cdot \|\hat{\mathbf{C}}_{k_{\Delta t}}\|_{\mathbf{F}}^2}}, \quad (6)$$

where $\langle \mathbf{A}, \mathbf{B} \rangle_{\mathbf{F}} = \sum_{i,j} A[i, j]B[i, j]$ and $\|\mathbf{A}\|_{\mathbf{F}} = \sqrt{\langle \mathbf{A}, \mathbf{A} \rangle_{\mathbf{F}}}$ are the Frobenius inner product and Frobenius norm, respectively. k_t and $k_{\Delta t}$ denote the time indices of the reference and shifted LSF, respectively. Collinearity is a bounded metric with values between 0 and 1, where 1 indicates identical and 0 completely dissimilar matrices. For the evaluation we define the channel stationary, as the time duration over which collinearity is above the defined cut-off value

$$t_{\text{stat}}[k_t] = (N + (k_{\Delta t} - 1)\Delta_t)T_s, \quad \forall k_{\Delta t} : \gamma^{(t)}[k_t, k_{\Delta t}] > 0.9. \quad (7)$$

4 Results

In order to establish a comparable movement representation across different velocities, we define $\alpha \triangleq (k_t - 0.5)\Delta_t T_s$ and $\Delta\alpha \triangleq (k_{\Delta t} - 0.5)\Delta_t T_s$. They denote the angular center position on the arc (Fig. 1) of each reference and time-shifted LSF. As explained in Section 3, choosing the size of the LCTF is a trade-off between the accuracy of the stationarity evaluation and the LSF Doppler resolution. On one side, choosing a higher value of N can jeopardize the assumption of stationarity over one LCTF. On the other side, by setting N lower, we decrease the LSF Doppler resolution. With an increased velocity of the TX, Doppler shift increases proportionally. By setting the same angular movement, over which the LCTF is defined, we achieve the same LSF Doppler resolution compared to the maximal Doppler shift, for both velocities. At the frequency band 25.5 GHz we set $N = 25$ for both velocities, which corresponds to 4° rotary arm angular movement. For all evaluations presented in this paper, we keep the LCTF time shift $\Delta_t = 2$, corresponding to 0.32° of angular resolution.

Fig. 2 shows the stationarity evaluation for $f_c = 25.5$ GHz. The diagonal shows the collinearity of the LSF to itself. As we move along the x-axis, away from the diagonal, we compare the LSF with the following LSFs in the time domain. Observing the stationarity evaluation for 25.5 GHz frequency band for a TX velocity of 40 km/h (Fig. 2a) and 100 km/h (Fig. 2b) we notice their high similarity in the spatial stationarity distribution. Fig. 3 shows the comparison of stationarity time between different velocities. For a fair comparison in the time domain, we set the same LCTF time length of 2.5 ms for both velocities. We notice that the stationarity time peaks, visible at lower velocities, are scaled down, with increased velocity.

Further, we evaluate the stationarity time for the frequency band 2.55 GHz. Because the Doppler shift is proportional to the center frequency, sub-6 GHz experiences a much lower Doppler shift compared to mmWave. Therefore, in order to maintain the Doppler resolution high, we increase the length of the LCTF at the cost of spatial resolution. We set $N = 100$, corresponding to 16° of angular movement. First, we observe larger stationarity regions compared to the mmWave channels. Secondly, we notice similarities between the two frequency bands:

- low stationarity regions at $\alpha < -27^\circ$ and $14^\circ < \alpha < 25^\circ$, and
- large stationarity regions $-27^\circ < \alpha < 14^\circ$ and $\alpha > 25^\circ$.

These similarities between the sub-6 GHz and mmWave band can be explained by the fact, shown in the recent literature, that significant scatterers are visible in both frequency bands [13, 14, 15].

5 Conclusion

In this paper we evaluated stationarity regions of measured high-mobility multi-band wireless channels. We defined

the stationarity region as the maximal time duration, over which the local scattering function (LSF) stays approximately constant.

The measurement campaign was performed in a controlled lab environment. Such an environment enabled us to perform repeatable measurements and show the influence of the specific parameters. We demonstrated the high similarity of stationarity in the spatial domain when comparing the scenarios where the transmitter was moving at different velocities. Further, that means that the stationarity time is scaled down with an increased velocity. Moreover, we demonstrated the similarities in spatial stationarity between the sub-6 GHz and millimeter wave (mmWave) wireless channels. Nevertheless, we showed that the sub-6 GHz channels are characterized by larger stationarity regions in the time domain.

References

- [1] G. Matz, "Doubly underspread non-WSSUS channels: analysis and estimation of channel statistics," in *2003 4th IEEE Workshop on Signal Processing Advances in Wireless Communications - SPAWC 2003 (IEEE Cat. No.03EX689)*, 2003, pp. 190–194.
- [2] —, "On non-WSSUS wireless fading channels," *IEEE Transactions on Wireless Communications*, vol. 4, no. 5, pp. 2465–2478, 2005.
- [3] A. Paier *et al.*, "Non-WSSUS vehicular channel characterization in highway and urban scenarios at 5.2GHz using the local scattering function," in *2008 International ITG Workshop on Smart Antennas*, 2008, pp. 9–15.
- [4] L. Bernadó, T. Zemen, F. Tufvesson, A. F. Molisch, and C. F. Mecklenbräuker, "The (in-) validity of the WSSUS assumption in vehicular radio channels," in *2012 IEEE 23rd International Symposium on Personal, Indoor and Mobile Radio Communications - (PIMRC)*, 2012, pp. 1757–1762.
- [5] —, "Delay and doppler spreads of nonstationary vehicular channels for safety-relevant scenarios," *IEEE Transactions on Vehicular Technology*, vol. 63, no. 1, pp. 82–93, 2014.
- [6] R. He *et al.*, "Characterization of quasi-stationarity regions for vehicle-to-vehicle radio channels," *IEEE Transactions on Antennas and Propagation*, vol. 63, no. 5, pp. 2237–2251, 2015.
- [7] J.-J. Park, J. Lee, K.-W. Kim, M.-D. Kim, H.-K. Kwon, and K. C. Lee, "Wide-sense stationarity of millimeter wave expressway channels based on 28 GHz measurements," in *2019 IEEE 90th Vehicular Technology Conference (VTC2019-Fall)*, 2019, pp. 1–5.
- [8] D. Radovic, H. Groll, and C. F. Mecklenbräuker, "Evaluation of stationarity regions in

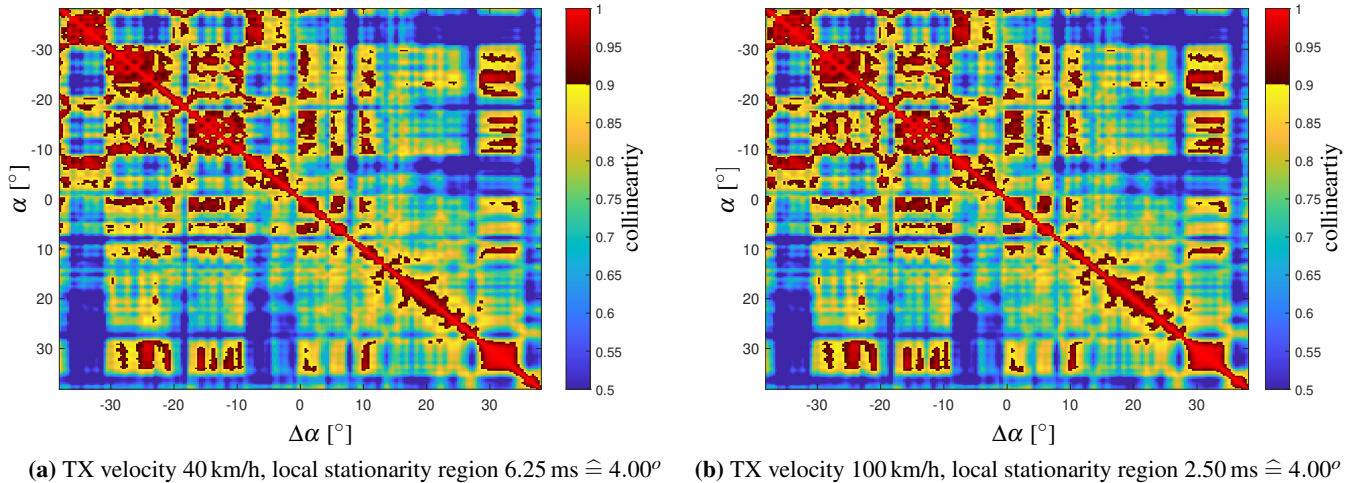


Figure 2. Stationarity evaluation for $f_c = 25.5 \text{ GHz}$, $B=100 \text{ MHz}$.

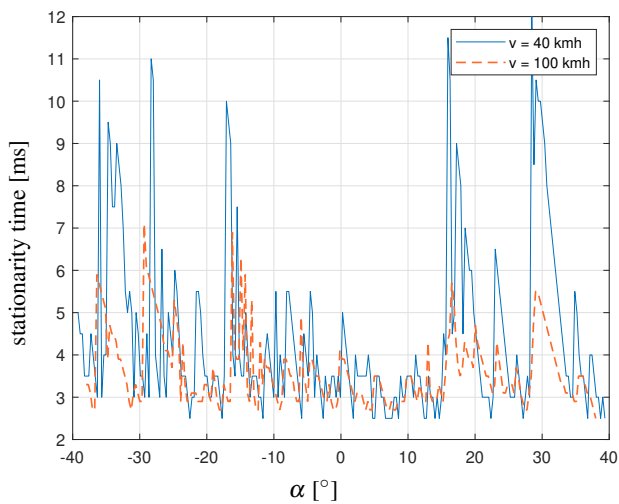


Figure 3. Stationarity time for $f_c = 25.5 \text{ GHz}$; TX velocity 40 vs. 100 km/h; local stationarity region 2.50 ms.

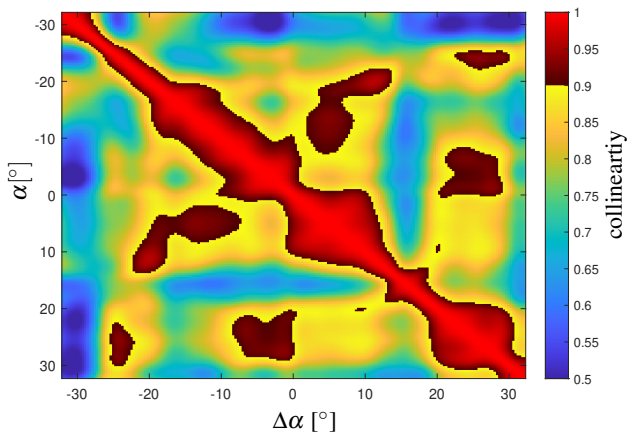


Figure 4. Stationarity evaluation for $f_c = 2.55 \text{ GHz}$; TX velocity 100 km/h, local stationarity region $10.00 \text{ ms} \hat{=} 16.00^\circ$.

measured non-WSSUS 60 GHz mmWave V2V channels,” pp. 1–5, 2022. [Online]. Available: <https://arxiv.org/abs/2210.02923>

- [9] Y. Tan, C.-X. Wang, J. O. Nielsen, and G. F. Pedersen, “Comparison of stationarity regions for wireless channels from 2 GHz to 30 GHz,” in *2017 13th International Wireless Communications and Mobile Computing Conference (IWCMC)*, 2017, pp. 647–652.
- [10] F. Pasic *et al.*, “Comparison of sub 6 GHz and mmWave wireless channel measurements at high speeds,” in *2022 16th European Conference on Antennas and Propagation (EuCAP)*, 2022, pp. 1–5.
- [11] —, “High-mobility wireless channel measurements at 5.9 GHz in an urban environment,” in *2022 International Balkan Conference on Communications and Networking (BalkanCom)*, 2022, pp. 100–104.
- [12] D. Slepian, “Prolate spheroidal wave functions, Fourier analysis, and uncertainty-V: The discrete case,” *Bell Syst. Techn J.*, vol. 57, no. 5, pp. 1371–1430, May 1978.
- [13] D. Dupleich *et al.*, “Multi-band propagation and radio channel characterization in street canyon scenarios for 5G and beyond,” *IEEE Access*, vol. 7, pp. 160 385–160 396, 2019.
- [14] M. Boban *et al.*, “Multi-band vehicle-to-vehicle channel characterization in the presence of vehicle blockage,” *IEEE Access*, vol. 7, pp. 9724–9735, 2019.
- [15] M. Hofer *et al.*, “Wireless vehicular multiband measurements in centimeterwave and millimeterwave bands,” in *2021 IEEE 32nd Annual International Symposium on Personal, Indoor and Mobile Radio Communications (PIMRC)*, 2021, pp. 836–841.